UNCERTAINTY vs PERFORMANCE TRADE-OFFS IN ROBUST FEEDBACK CONTROL: A MIMO CASE STUDY

J.F. Vasconcelos[†], M. Athans[†*], S. Fekri[†**], C. Silvestre[†] and P. Oliveira[†]

***Abstract*— We use a non-trivial MIMO three-cart Mass-Spring-Dashpot (MSD) system to demonstrate how performance (disturbance-rejection) is reduced as the level of uncertainty in one or two real parameters is increased in the presence of unmodeled dynamics. All designs are carried out by the mixed-μ robust synthesis methodology. Comparisons are made (a) in the frequency-domain, (b) by RMS values of key signals and (c) in time-domain simulation results.**

I. INTRODUCTION

All LTI models of real dynamic systems are subject to uncertainty. For each LTI model we must take into account unmodeled dynamics and uncertain real parameters, as well as unmeasurable exogenous plant disturbances and sensor noise. The design of a MIMO dynamic compensator, and of the resulting robust feedback system, must possess guarantees of both stability-robustness and performance-robustness to the explicit performance specifications posed by the control system designer.

Fortunately, in the past decade or so, the mixed-μ design methodology [4], [5] and MATLAB software [1], utilizing the so-called D,G-K iteration, have been developed that can indeed be used to design robust MIMO feedback control systems with the requisite stability- and performance-robustness guarantees. However, there is a scarcity of complex MIMO numerical studies that demonstrate the very important trade-offs between performance and uncertainty. One of the possible reasons is that the commercial version of the Robust Toolbox [1] in MATLAB does not fully implement the complete mixed-μ compensator design process.

In this paper we use two-input two-output (TITO) Mass-Spring-Dashpot (MSD) test example to illustrate key performance vs uncertainty trade-offs. We have used a "beta" version of the mixed-μ software (provided to us by Prof. Gary Balas) which fully implements the mixed-μ D,G-K iteration, leading to the best possible robust compensator. Of course, since we deal with a MIMO design, "directional properties" quantified by the Singular Value Decomposition (SVD) are also important. A similar study [3] examined similar trade-offs for a simpler SISO MSD example.

Loosely speaking, the mixed-μ compensator design process "detunes" an optimal $\mathcal{H}_\infty$ compensator, designed for the nominal plant, to hedge for the uncertain real parameters. The greater the parametric uncertainty the smaller the guaranteed performance. In this study we shall focus upon the deterioration of disturbance-rejection as the parametric uncertainty increases.

The paper is organized as follows. In Section II we discuss the MSD dynamics, uncertain real parameters, unmodeled dynamics and the open-loop frequency-domain analysis. In Section III we present the specific performance specifications using frequency-domain weights; we also define two cases, one involving a single uncertain parameter (a spring stiffness) and another that, in addition, involves an uncertain mass. In this manner, we can examine the performance deterioration when we add another uncertain real parameter, in terms of performance weights, disturbance-rejection and output RMS tables. In Section IV we discuss the characteristics of the robust compensators, obtained by the mixed-μ method, in the frequency-domain. The trade-offs in terms of frequency domain disturbance-rejection SVD plots are also presented. In Section V we show time-transients which also illustrate the deterioration in disturbance-rejection as the parametric uncertainty increases. Section VI presents some brief conclusions.

II. PLANT MODEL

The Mass-Spring-Dashpot (MSD) system, depicted in Fig. 1, is composed by three masses, denoted by m_1, m_2 and m_3, interconnected by elastic springs and dashpots elements, whose stiffness and damping coefficients are denoted by k_1, k_2, k_3, and b_1, b_2, b_3, respectively. The control inputs u_1 and u_2 are applied to masses m_1 and m_3, respectively, and are affected by an unknown bounded pure time-delay.

Position sensors y_1 and y_2, corrupted by measurement noises θ_1 and θ_2, are included on masses m_2 and m_3. The performance outputs positions z_1 and z_2 are defined on masses m_2 and m_3 in order to minimize their displacements. From the system configuration, it is immediate that the control is partially non-collocated because of the performance specifications represented by z_1. The two disturbances d_1 and d_2 act on the same masses where the performance outputs are defined, and thus d_1 cannot be directly compensated by a control input.

[†] The authors are with the Institute for Systems and Robotics (ISR), Instituto Superior Técnico, Lisbon, Portugal. E-mails: {jfvasconcelos, athans, cjs, pjcro}@isr.ist.utl.pt
Tel: (+351) 21-8418054, Fax: (+351) 21-8418291.

[*] M. Athans is also Professor of EECS (emeritus), M.I.T., USA.

[**]S. Fekri is now Research Associate in Department of Engineering, Control & Instrumentation Research Laboratory, University of Leicester, Leicester LE1 7RH, UK. E-mail: sf111@le.ac.uk.

This work was partially supported by Fundação para a Ciência e a Tecnologia (ISR/IST plurianual funding) through the POS_Conhecimento Program that includes FEDER funds. The work of J.F. Vasconcelos was supported by a PhD Student Scholarship, SFRH/BD/18954/2004, from the Portuguese FCT POCTI programme.

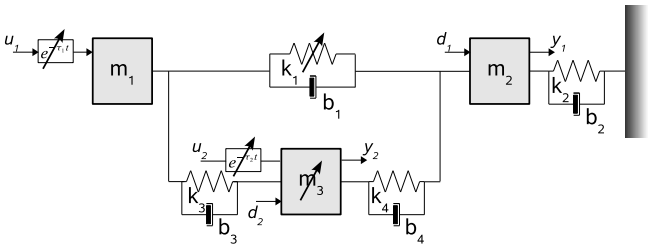

Fig. 1. Mass-Spring-Dashpot system

A. System Dynamics

Based on Newton's laws, the MSD plant dynamics are derived to yield the augmented state model

$$\begin{bmatrix}\dot{\mathbf{x}}(t)\\ \dot{\mathbf{v}}(t)\end{bmatrix} = \begin{bmatrix}\mathbf{0} & \mathbf{I}_{3\times3}\\ \mathbf{A}_{21} & \mathbf{A}_{22}\end{bmatrix}\begin{bmatrix}\mathbf{x}(t)\\ \mathbf{v}(t)\end{bmatrix} + \begin{bmatrix}\mathbf{0}\\ \mathbf{B}_1\end{bmatrix}\mathbf{d}(t) + \begin{bmatrix}\mathbf{0}\\ \mathbf{B}_2\end{bmatrix}\mathbf{u}(t) \quad (1)$$

where the state variables $\mathbf{x}(t)$, state noise $\mathbf{d}(t)$ and inputs $\mathbf{u}(t)$ are described by

$$\begin{aligned}\mathbf{x}(t) &= \begin{bmatrix}x_1(t) & x_2(t) & x_3(t)\end{bmatrix}^T, \mathbf{d}(t) = \begin{bmatrix}d_1(t) & d_2(t)\end{bmatrix}^T\\ \mathbf{v}(t) &= \begin{bmatrix}v_1(t) & v_2(t) & v_3(t)\end{bmatrix}^T, \mathbf{u}(t) = \begin{bmatrix}u_1(t) & u_2(t)\end{bmatrix}^T\end{aligned} \quad (2)$$

the state model matrices are stationary and given by

$$\begin{aligned}\mathbf{A}_{21} &= \begin{bmatrix}-\frac{k_1+k_3}{m_1} & \frac{k_1}{m_1} & \frac{k_3}{m_1}\\ \frac{k_1}{m_2} & -\frac{k_1+k_2+k_4}{m_2} & \frac{k_4}{m_2}\\ \frac{k_3}{m_3} & \frac{k_4}{m_3} & -\frac{k_3+k_4}{m_3}\end{bmatrix}\\ \mathbf{A}_{22} &= \begin{bmatrix}-\frac{b_1+b_3}{m_1} & \frac{b_1}{m_1} & \frac{b_3}{m_1}\\ \frac{b_1}{m_2} & -\frac{b_1+b_2+b_4}{m_2} & \frac{b_4}{m_2}\\ \frac{b_3}{m_3} & \frac{b_4}{m_3} & -\frac{b_3+b_4}{m_3}\end{bmatrix}\\ \mathbf{B}_1 &= \begin{bmatrix}0 & 0\\ \frac{1}{m_2} & 0\\ 0 & \frac{1}{m_3}\end{bmatrix}, \quad \mathbf{B}_2 = \begin{bmatrix}\frac{1}{m_1} & 0\\ 0 & 0\\ 0 & \frac{1}{m_3}\end{bmatrix}\end{aligned} \quad (3)$$

and m_i, x_i and v_i are the mass, position and velocity of the mass indexed by $i = 1, 2, 3$, k_i and b_i are the elastic and damping coefficients and u_i and d_i are the forces and disturbances acting on the system, respectively.

The state performance output $\mathbf{z}(t)$ is defined on $x_2(t)$ and $x_3(t)$. The performance state variables are monitored by position sensors $\mathbf{y}(t)$ corrupted by additive noise

$$\begin{aligned}\mathbf{z}(t) &= \begin{bmatrix}x_2(t)\\ x_3(t)\end{bmatrix}, \quad \mathbf{y}(t) = \mathbf{z}(t) + \begin{bmatrix}\theta_{w\,1}(t)\\ \theta_{w\,2}(t)\end{bmatrix}\\ \mathbf{z}_{px}(t) &= \mathbf{W}_{px}\mathbf{z}(t), \quad \mathbf{z}_{pu}(t) = \mathbf{W}_{pu}\mathbf{u}(t)\end{aligned} \quad (4)$$

where $\mathbf{z}_{px}(t)$ and $\mathbf{z}_{pu}(t)$ are performance vectors, $\mathbf{W}_{px}$ and $\mathbf{W}_{pu}$ are performance weights and $\boldsymbol{\theta}_w(t)$ is the measurement noise.

For the current case, the known physical parameters are

$$\begin{aligned}&m_1 = m_2 = 1\,\text{Kg}, \quad b_1 = b_2 = b_3 = b_4 = 0.05\,\text{Ns/m}\\ &k_2 = 0.15\,\text{N/m},\ k_3 = 1.00\,\text{N/m},\ k_4 = 0.20\,\text{N/m}\end{aligned} \quad (5)$$

B. System Disturbances

The state disturbances are modeled as low-frequency colored noise generated by a prewhitening process

$$\begin{aligned}\mathbf{d}(s) &= \mathbf{W}_d(s)\boldsymbol{\xi}(s)\\ \mathbf{W}_d(s) &= \frac{\alpha}{s+\alpha}\mathbf{I}_{2\times2}\end{aligned} \quad (6)$$

where α is the cut-off frequency and $\boldsymbol{\xi}(s)$ is a zero-mean, Gaussian white noise, with unit intensity $\Xi = \mathbf{I}_{2\times2}$. The cut-off frequency is set to $\alpha = 2$ rad/sec.

The measurement noise $\boldsymbol{\theta}_w(t)$ is a zero-mean, Gaussian white noise with covariance given by

$$\begin{aligned}\boldsymbol{\theta}_w(s) &= \mathbf{W}_\theta(s)\boldsymbol{\theta}(s)\\ \mathbf{W}_\theta(s) &= \begin{bmatrix}\Theta_{11}^{\frac{1}{2}} & 0\\ 0 & \Theta_{22}^{\frac{1}{2}}\end{bmatrix}\end{aligned} \quad (7)$$

where $\Theta_{11} = \Theta_{22} = 10^{-6}$ and $\boldsymbol{\theta}(s)$ is a zero-mean, Gaussian white noise, with unit intensity.

C. Uncertain Parameters

As shown in Fig. 1, the plant includes two uncertain parameters in the control time delay, given by time constants τ_1 and τ_2, and two other associated to mass m_3 and the elastic coefficient k_1 values. These are modeled according to the mixed-μ synthesis methodology, resorting to either structured or unstructured models.

1) Structured Uncertainty: The structured uncertain parameters k_1 and m_3 are described by

$$k_1 = \bar{k}_1 + \delta_{k_1}\tilde{k}_1 \quad (8)$$

$$m_3 = \bar{m}_3 + \delta_{m_3}\tilde{m}_3 \quad (9)$$

where $\bar{k}_1$ and $\bar{m}_3$ are the nominal values, $\tilde{k}_1$ and $\tilde{m}_3$ are the uncertainty levels and the variables $\delta_{k_1} \in \mathbb{R}$ and $\delta_{m_3} \in \mathbb{R}$ determine the structured uncertainties values and satisfy $\|\delta_{k_1}\| \leq 1$ and $\|\delta_{m_3}\| \leq 1$. The parametric uncertainties are described in the system in the form of lower loop LFT transfer function [1].

The structured uncertain parameters values are

$$\begin{aligned}&k_1 \in \begin{bmatrix}0.25 & 1.75\end{bmatrix}\ \text{N/m} \rightarrow \bar{k}_1 = 1\,\text{N/m}, \tilde{k}_1 = 0.75\,\text{N/m}\\ &m_3 \in \begin{bmatrix}0.20 & 1.80\end{bmatrix}\ \text{Kg} \rightarrow \bar{m}_3 = 1\,\text{Kg}, \tilde{m}_3 = 0.8\,\text{Kg}\end{aligned} \quad (10)$$

2) Unstructured Uncertainty: The control channels pure time-delays are infinite-dimensional systems, so they cannot be modeled by a finite number of state variables. Assuming that the time-delays are neglected, the resulting multiplicative error is $e_M(s) = e^{-s\tau} - 1$.

The multiplicative error magnitude can be approximated by an upper bound high-pass transfer function $\mathbf{W}_{\tau i}(s)$ with a pole placed near the frequency $\omega = \frac{\pi}{\tau_i}$. For the μ-synthesis methodology, the magnitude and phase of the transfer function $\mathbf{W}_{\tau i}(s)$ are shaped by a delta block $\Delta_{\tau i}(s) \in \mathbb{C}$ that satisfies $\|\Delta_{\tau i}(s)\|_\infty \leq 1$ and introduces a phase uncertainty in the range of $\pm 180\,^\circ$.

The control channel time-delays upper bounds are

$$\tau_i \leq 0.03\,\text{s}, \quad i = 1, 2 \quad (11)$$

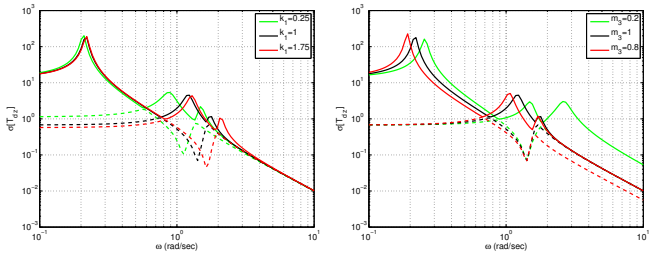

(a) Varying k_1, nominal m_3 (b) Nominal k_1, varying m_3

Fig. 2. Open-loop disturbance to output singular values, $T_{dy}(s)$

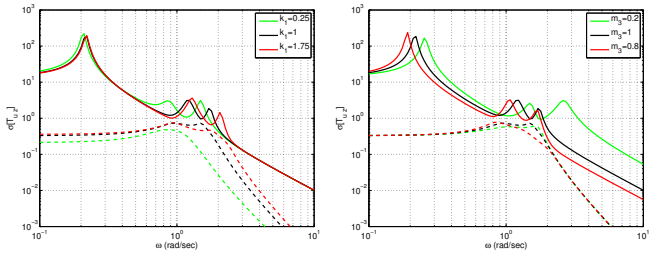

(a) Varying k_1, nominal m_3 (b) Nominal k_1, varying m_3

Fig. 3. Open-loop control to output singular values, $T_{uy}(s)$

so the $\mathbf{W}_{\tau i}(s)$ transfer function pole is set near the maximum time-delay frequency and the gain adjusts the upper bound magnitude to the $e_M(s)$ transfer function. The frequency weight block is defined as

$$\begin{aligned} \mathbf{z}_\tau(s) &= \mathbf{W}_\tau(s)\mathbf{u}(s) \\ \mathbf{W}_\tau(s) &= 2.1\frac{s}{s+40}\mathbf{I}_{2\times 2} \end{aligned} \tag{12}$$

D. Frequency Domain Analysis

The singular values of the disturbance and control to state performance transfer functions, $T_{dy}(s)$ and $T_{uy}(s)$ respectively, are presented in Fig. 2 and Fig. 3. As expected, increasing the spring stiffness k_1 or decreasing mass coefficient m_3 will open the system bandwidth, and vice-versa. The zeros in Fig. 2 reflect the placement of disturbances in the masses where sensors are installed. The absence of zeros in Fig. 3 evidences the fact that control input $u_1(t)$ is not collocated on a mass associated with the performance vector.

For the problem at hand, the system amplifies the frequencies where $\mathbf{d}(s)$ has more power, $\omega < 2$ rad/sec. Therefore, the open-loop dynamics naturally amplify the disturbance and the controller must change the directionality of the closed-loop system to properly filter out the disturbance effects in the output vector.

III. PERFORMANCE-ROBUSTNESS

The performance-robustness and stability-robustness requirements are introduced in the generalized plant, shown in Fig. 4, under the form of frequency weights. The performance-robustness requirements are introduced using frequency weights in the output variables, whereas the stability-robustness specifications are associated to the weights defined in Section II.

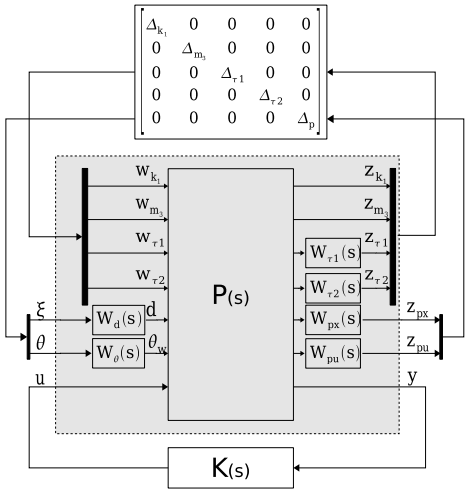

Fig. 4. Generalized plant

This section details the performance-robustness specifications and the mixed-μ synthesis setup to find the best performance given the parametric uncertainty interval. The influence of the number of uncertainties and the impact of uncertainty levels $\tilde{k}_1$ and $\tilde{m}_3$ in the system performance are discussed.

A. Performance Specifications

The disturbance must be rejected, as much as possible, in the closed-loop system. The state performance weights, defined on mass 2 and mass 3 positions, introduce good disturbance-rejection in the frequency range where the disturbance $\mathbf{d}(s)$ has most of its power

$$\mathbf{W}_{px}(s) = \frac{A_p\alpha}{s+\alpha}\begin{bmatrix} A_1 & 0 \\ 0 & A_2 \end{bmatrix} \tag{13}$$

where $\alpha = 2$ rad/sec and A_1 and A_2 shape the directionality of the system. The A_p performance weight reflects the best possible disturbance-rejection and is determined in the μ-synthesis procedure.

The controller inputs power is available at low frequencies but actuation is expensive at high frequencies

$$\mathbf{W}_{pu}(s) = \frac{10(s+10^2)}{s+10^6}\mathbf{I}_{2\times 2} \tag{14}$$

The controller specifications (14) limit the bandwidth of the closed-loop system.

As detailed in [2], the performance-robustness specifications are satisfied by introducing an additional performance delta block $\Delta_p(s)$ in the μ-synthesis methodology.

B. Mixed-μ Synthesis Setup

The μ-synthesis is applied to find the largest possible performance weight A_p for the MSD plant, thus yielding the best disturbance-rejection possible. Based on the experience drawn from extensive simulations, the singular structured value μ upper bound, denoted by $\bar{\mu}$, is considered to monotonically increase with the performance weight A_p.

TABLE I

D,G-KIT PERFORMANCE RESULTS (k_1 UNCERTAIN, $A_1 = A_2$)

$\tilde{k}_1$	A_p	$\|T_{\xi z}(0)\|$	$RMS(z_1)$	$RMS(z_2)$
0.75	23.28	3.51×10^{-2}	1.40×10^{-2}	3.51×10^{-2}
0.50	63.80	1.44×10^{-2}	1.04×10^{-2}	2.27×10^{-2}
0.25	134.93	7.18×10^{-3}	7.80×10^{-3}	8.24×10^{-3}
≈ 0	223.25	4.27×10^{-3}	7.63×10^{-3}	1.22×10^{-2}

Using the bisection search algorithm, the adopted procedure tries to find the largest A_p such that the norm of the smallest destabilizing structured uncertainty is greater than unity [2], i.e., $\bar{\mu} < 1$. In other words, given the uncertainty blocks defined in Sections II and III-A, there is no valid $\Delta(s)$ that destabilizes the system. The D-K and D,G-K iterations are run by the `dgit` and `dgkit` commands included in the Robust Control Toolbox of Matlab 7.1 [1] and in the beta version software package kindly provided by Prof. Gary Balas.

The μ-synthesis properties are studied by varying the number of parametric uncertainties and their uncertainty level, represented by $\tilde{k}_1$ and $\tilde{m}_3$. Also, the performance weights A_1 and A_2 relative values are modified to evidence directionality aspects with respect to the nominal setting $A_1 = A_2 = 1$.

C. Performance-Robustness Results

1) Single Parametric Uncertainty: The performance results for a parametric spring stiffness uncertainty k_1, computed for the worst-case disturbance, are detailed in Table I. The norm $\|\|$ denotes the maximum singular value at DC. It is obvious that smaller uncertainty levels $\tilde{k}_1$ yield better output performance weight A_p. That is, if the stability-robustness specifications are less demanding, then better performance-robustness specifications are obtained, and the closed-loop will yield better disturbance-rejection and command-following.

The values of the state performance weight A_p are not linear with respect to $\tilde{k}_1$, as depicted in Fig. 5. As the uncertainty level $\tilde{k}_1$ grows, the control problem becomes harder and A_p tends to zero, which means that it is not possible to achieve performance-robustness with essentially unknown dynamics.

The disturbance-rejection gain for low frequencies $\|T_{\xi z}(0)\|$ decreases with the uncertainty and is about $\frac{1}{A_p}$, as expected. The RMS value of the mass positions $x_2(t)$ and $x_3(t)$ tends to decrease, reflecting better performance-robustness. In spite of this tendency, μ-synthesis is designed using an $\mathcal{H}_\infty$ control methodology, so it is not mandatory that the performance vector $\mathcal{H}_2$ norm (i.e. RMS) decreases as the uncertainty level $\tilde{k}_1$ becomes smaller.

The performance-robustness results for asymmetric performance weights cases $(A_1 = 5, A_2 = 1)$ and $(A_1 = 1, A_2 = 5)$ are detailed in Tables II and III, respectively.

The problem of non-collocated control makes mass 2 position harder to control, so the performance specification associated to $z_1(t)$ is more difficult satisfy than for $z_2(t)$.

TABLE II

D,G-KIT PERFORMANCE RESULTS (k_1 UNCERTAIN, $A_1 = 5, A_2 = 1$)

$\tilde{k}_1$	A_p	$\|T_{\xi z}(0)\|$	$RMS(z_1)$	$RMS(z_2)$
0.75	4.93	0.101	1.35×10^{-2}	7.58×10^{-2}
0.50	12.71	4.77×10^{-2}	9.56×10^{-3}	3.81×10^{-2}
0.25	26.04	2.32×10^{-2}	7.98×10^{-3}	2.35×10^{-2}
≈ 0	45.60	1.06×10^{-2}	7.51×10^{-3}	2.60×10^{-2}

TABLE III

D,G-KIT PERFORMANCE RESULTS (k_1 UNCERTAIN, $A_1 = 1, A_2 = 5$)

$\tilde{k}_1$	A_p	$\|T_{\xi z}(0)\|$	$RMS(z_1)$	$RMS(z_2)$
0.75	13.43	2.22×10^{-2}	2.11×10^{-2}	2.42×10^{-2}
0.50	39.25	1.42×10^{-2}	1.31×10^{-2}	1.73×10^{-2}
0.25	88.40	8.56×10^{-3}	1.03×10^{-2}	3.66×10^{-3}
≈ 0	135.85	6.91×10^{-3}	1.10×10^{-2}	5.52×10^{-3}

Consequently, the performance weight A_p for $A_1 = 5A_2$ is lower than for $A_2 = 5A_1$, while the disturbance-rejection at low frequencies $\|T_{\xi z}(0)\|$ is more efficient for $A_2 = 5A_1$ than for $A_1 = 5A_2$.

The complex-μ synthesis is applied using the D-K iterations, i.e. the version in the commercially available MATLAB software [1], to find the best A_p such that $\bar{\mu} < 1$ and $\delta_{k_1} \in \mathbb{C}$. As shown in Table IV, this methodology yields very conservative results. The real parametric uncertainties play a major role in the system dynamics, thus requiring the D,G-K algorithm approach for good performance results. For very small uncertainty levels ($\tilde{k}_1 \approx \tilde{m}_3 \approx 0$), the D-K and D,G-K performance results are similar, as expected.

2) Two Parametric Uncertainties: The performance weight A_p and low-frequency disturbance-rejection $\|T_{\xi z}(0)\|$ for parametric uncertainties in spring stiffness k_1 and mass coefficient m_3 are shown in Table V and Table VI.

TABLE IV

D-KIT VS D,G-KIT PERFORMANCE (k_1 UNCERTAIN, $\tilde{k}_1 = 0.75$)

	D-Kit		**D,G-Kit**	
	A_p	$\|T_{\xi z}(0)\|$	A_p	$\|T_{\xi z}(0)\|$
$A_1 = 1, A_2 = 1$	5.31	0.123	23.28	3.51×10^{-2}
$A_1 = 5, A_2 = 1$	1.15	0.279	4.93	0.101
$A_1 = 1, A_2 = 5$	5.37	8.70×10^{-2}	13.43	2.22×10^{-2}

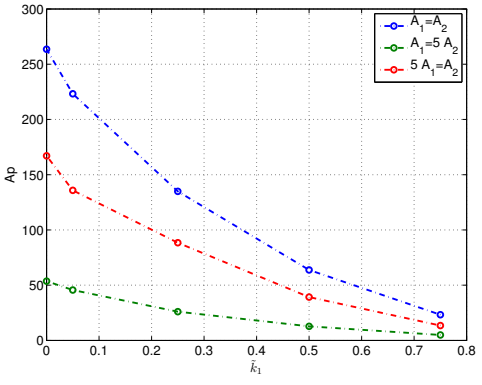

Fig. 5. Performance weight A_p *vs* uncertainty level $\tilde{k}_1$ (only k_1 uncertain)

TABLE V

D,G-KIT PERFORMANCE WEIGHT A_p (k_1, m_3 UNCERTAIN, $A_1 = A_2$)

$\tilde{m}_3$	$\tilde{k}_1$			
	0.75	0.50	0.25	≈ 0
0.80	15.27	42.79	47.19	62.40
0.50	18.95	57.44	127.18	204.12
0.20	20.90	62.85	130.92	216.15
≈ 0	22.98	63.90	134.56	221.62

TABLE VI

D,G-KIT LOW-FREQUENCY DISTURBANCE-REJECTION $\|T_{\xi z}(0)\|$ (k_1, m_3 UNCERTAIN, $A_1 = A_2$)

$\tilde{m}_3$	$\tilde{k}_1$			
	0.75	0.50	0.25	≈ 0
0.80	6.42×10^{-2}	2.27×10^{-2}	1.79×10^{-2}	1.59×10^{-2}
0.50	4.94×10^{-2}	1.70×10^{-2}	7.70×10^{-3}	4.76×10^{-3}
0.20	4.06×10^{-2}	1.52×10^{-2}	7.41×10^{-3}	4.42×10^{-3}
≈ 0	3.61×10^{-2}	1.46×10^{-2}	7.05×10^{-3}	4.33×10^{-3}

Again, higher performance weights A_p are obtained when the uncertainty levels $\tilde{k}_1$ and $\tilde{m}_3$ are smaller. In particular, the A_p values for a very small uncertainty level $\tilde{m}_3 \approx 0$ are similar to those obtained in the single uncertainty k_1 case, see Table I versus Table V.

Adding a significant m_3 uncertainty clearly decreases the performance of the system, as expected, and only for small $\tilde{m}_3$ the effect of adding one more uncertainty is not so dramatic.

As shown in Tables V and VI and depicted in Fig. 6(a), for $A_1 = A_2$ the performance weight A_p and the low-frequency disturbance-rejection $\|T_{\xi z}(0)\|$ are more influenced by the spring stiffness uncertainty $\tilde{k}_1$ than by the mass uncertainty $\tilde{m}_3$. Physically, this reflects the importance of the uncertainty k_1 in the non-collocated control problem, where the control input $u_1(t)$ influence on mass 2 position is performed mainly through spring 1.

The impact of m_3 uncertainty in the system performance becomes more noticeable for asymmetric weights $(A_1 = 1, A_2 = 5)$, as shown in Fig. 6(b) and presented in Table VII. In this case, the performance output gain A_2 shifts the control problem focus from mass 2 to the mass 3 position, so the importance of mass m_3 uncertainty in the closed-loop system performance is emphasized.

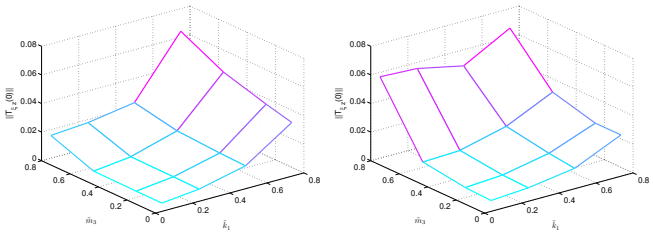

(a) $A_2 = A_1$ (b) $A_2 = 5A_1$

Fig. 6. Disturbance-rejection $\|T_{\xi z}(0)\|$ *vs* uncertainty level $(\tilde{k}_1, \tilde{m}_3)$

TABLE VII

D,G-KIT PERFORMANCE WEIGHT A_p (k_1, m_3 UNCERTAIN, $A_2 = 5A_1$)

$\tilde{m}_3$	$\tilde{k}_1$			
	0.75	0.50	0.25	≈ 0
0.80	4.85	11.63	13.75	15.87
0.50	9.47	30.96	64.39	84.45
0.20	13.81	41.09	90.51	135.89
≈ 0	14.63	43.02	99.26	153.03

IV. FREQUENCY-DOMAIN ANALYSIS

The disturbance to performance output closed-loop transfer function $T_{\xi z}(s)$ is depicted in Fig. 7(a). In the frequency domain, the performance-robustness specifications shape the closed-loop transfer function to yield good disturbance-rejection in the critical frequencies $\omega \in \begin{bmatrix} 0 & 2 \end{bmatrix}$ rad/sec, where $\mathbf{d}(s)$ has more power. Smaller uncertainty levels $\tilde{k}_1$ allow for better disturbance-rejection, as previously shown in Table I.

The transfer function performance degrades at high frequencies, due to the bandwidth increase that is closely related to improving low-frequency disturbance-rejection. Considering that the $\mathbf{d}(s)$ is modeled by low pass frequency weights (6), the controller synthesis methodology aims at finding the best controller for the frequencies where the disturbance has more power, at the cost of inflating the gains in the other frequency regions. If the disturbance is accurately modeled, this additional bandwidth does not produce actual performance degradation. Nonetheless, simulation results for generic disturbances are discussed in the ensuing.

The disturbance-rejection characteristics are also shown in the disturbance to control $T_{\xi u}(s)$ transfer function, see Fig. 7(b). The noise amplification is distinct in the frequency ranges $\omega \in \begin{bmatrix} 0 & 2 \end{bmatrix}$ rad/sec and $\omega > 2$ rad/sec. Reducing the uncertainty $\tilde{k}_1$ yields more disturbance influence in the control signal at low frequencies $\omega \in \begin{bmatrix} 0 & 2 \end{bmatrix}$ rad/sec.

The trade-off between stability-robustness and performance-robustness is clear in the compensator transfer function $K(s)$ presented in Fig. 7(c). The compensator gains are inflated for smaller uncertainties $\tilde{k}_1$, and according to the performance control weights $\mathbf{W}_{pu}(s)$ defined in (14), the control has most of its power located in the frequency range $\omega \in \begin{bmatrix} 0 & 10^6 \end{bmatrix}$ rad/sec. The poles located near the frequency $\omega = 10^2$rad/sec cut the compensator bandwidth where the zero of $\mathbf{W}_{pu}(s)$ starts to penalize the control signal, to finally attenuate the compensator power for $\omega > 10^6$rad/sec.

The stability- and performance-robustness characteristics also apply for the two uncertainty case, as shown in Fig. 8, for fixed $\tilde{k}_1$ and varying $\tilde{m}_3$.

The directionality of the system can be analyzed in Fig. 9. The compensator modifies the open-loop singular values and approximates the upper and lower singular value. Hence, performance vectors $z_1(t)$ and $z_2(t)$ tend to be equally influenced by the disturbance when the performance weights are similar $(A_1 = A_2)$, see Fig. 9(d).

In the case where the frequency weights introduce directionality, $A_1 = 5A_2$ or $A_2 = 5A_1$, the maximum singular

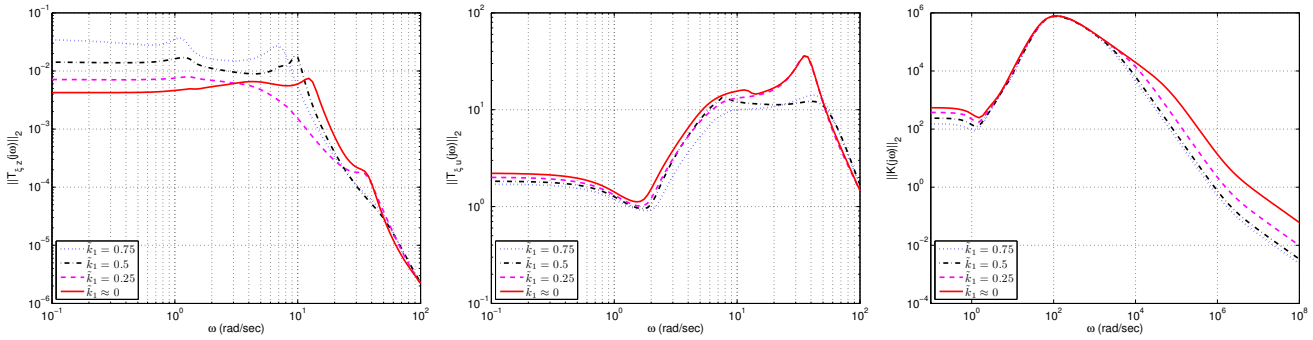

(a) $T_{\xi z}(s)$ (b) $T_{\xi u}(s)$ (c) $K(s)$

Fig. 7. Maximum singular value (only k_1 uncertain, $A_1 = A_2$)

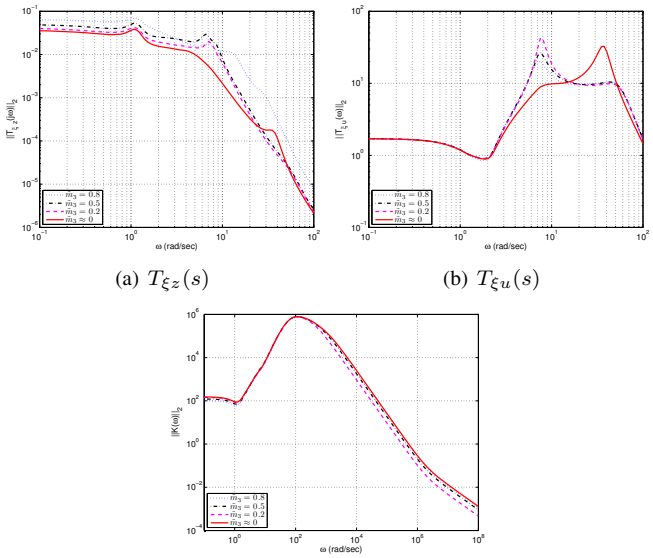

(a) $T_{\xi z}(s)$ (b) $T_{\xi u}(s)$

(c) $K(s)$

Fig. 8. Maximum singular value (k_1,m_3 uncertain, $\tilde{k}_1 = 0.75$, $A_1 = A_2$)

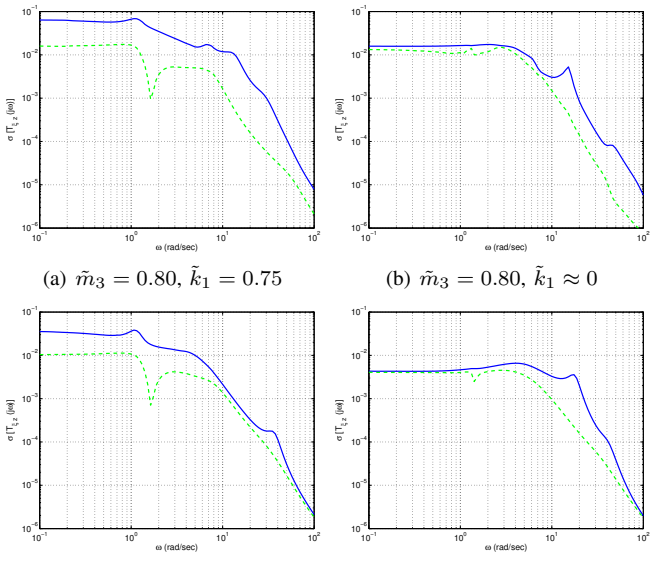

(a) $\tilde{m}_3 = 0.80$, $\tilde{k}_1 = 0.75$ (b) $\tilde{m}_3 = 0.80$, $\tilde{k}_1 \approx 0$

(c) $\tilde{m}_3 \approx 0$, $\tilde{k}_1 = 0.75$ (d) $\tilde{m}_3 \approx 0$, $\tilde{k}_1 \approx 0$

Fig. 9. Closed-loop $T_{\xi z}$ singular values (k_1, m_3 uncertain, $A_1 = A_2$)

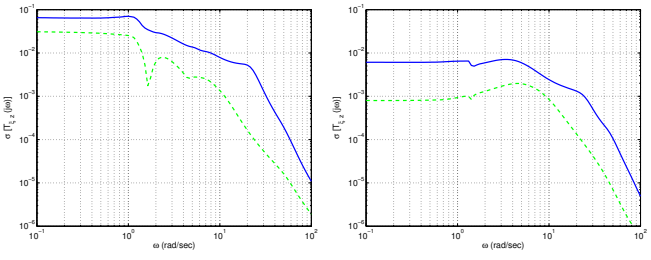

(a) $\tilde{m}_3 = 0.80$, $\tilde{k}_1 = 0.75$ (b) $\tilde{m}_3 \approx 0$, $\tilde{k}_1 \approx 0$

Fig. 10. Closed-loop $T_{\xi z}$ singular values (k_1, m_3 uncertain, $A_2 = 5A_1$)

values are approximately five times the value of the minimum singular value, as shown in Fig. 10.

Once again, Fig. 9 shows that changes in system performance-robustness are more influenced by the elastic coefficient uncertainty $\tilde{k}_1$ than by mass 3 uncertainty $\tilde{m}_3$ when $A_1 = A_2$.

V. TIME-DOMAIN SIMULATIONS

The generalized plant, shown in Fig. 4, was simulated to study the effects of unmodeled state disturbance in the system. It is assumed that the real control delay is $\tau_1 = \tau_2 = 5 \times 10^{-3}$ s and that the uncertain parameters are given by the nominal values $k_1 = \bar{k}_1, m_3 = \bar{m}_3$.

Although the disturbance is modeled by the frequency weight (6), in the time simulations the noise $\boldsymbol{\xi}(t)$ has an actual variance of $\Xi = 16\,\mathbf{I}_{2\times 2}$. The simulation results, depicted in Fig. 11, show that the controller is more efficient for smaller uncertainties, as expected. Mass position RMS values are according to the values predicted by analytical computations.

The RMS values of $u_1(t)$ and $u_2(t)$ are higher for small uncertainties, which agree with the results shown in Fig. 7(b) and Fig. 8(b). The directionality of the system is evidenced in Fig. 12 for (i) large $\tilde{k}_1$, small $\tilde{m}_3$ and (ii) small $\tilde{k}_1$, large $\tilde{m}_3$. For $A_2 = 5A_1$, the accuracy of mass m_3 parameter is more relevant to tackle performance output RMS values than the spring stiffness uncertainty k_1, as expected.

Applying a square-wave signal $\boldsymbol{\xi}(t)$ produces the disturbance $\mathbf{d}(t)$ depicted in Fig. 13 and yields the mass displacements shown in Fig. 14. Clearly, the smaller the

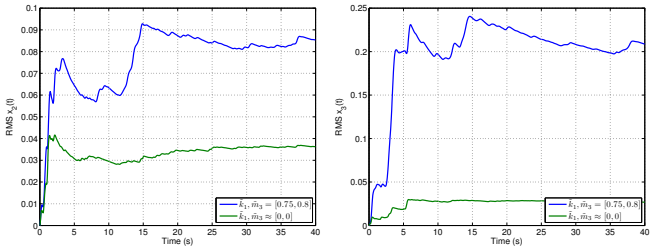

(a) Mass 2 position (b) Mass 3 position

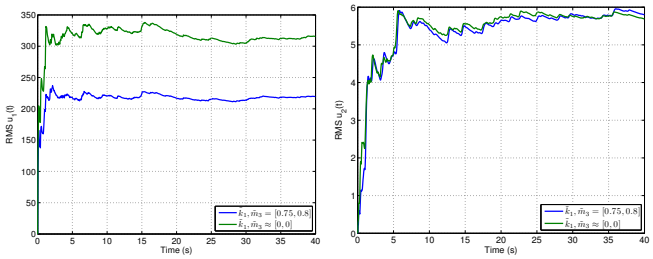

(c) Control input $u_1(t)$ (d) Control input $u_2(t)$

Fig. 11. RMS values (White-noise disturbance, $A_1 = A_2$)

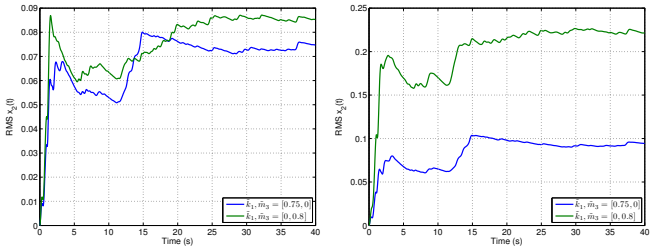

(a) Mass 2 position ($A_2 = A_1$) (b) Mass 2 position ($A_2 = 5A_1$)

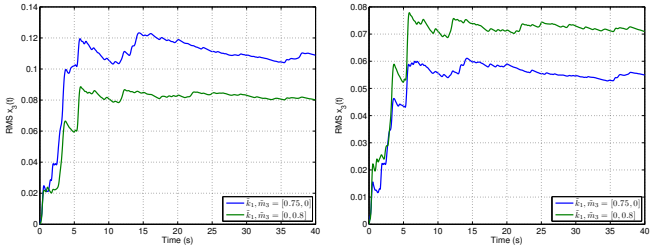

(c) Mass 3 position ($A_2 = A_1$) (d) Mass 3 position ($A_2 = 5A_1$)

Fig. 12. RMS values (White-noise disturbance)

uncertainty, the faster is the time response of the system. These time-domain results are according to the frequency-domain results discussed in Section IV.

VI. CONCLUSIONS

A robust compensator for a Mass-Spring-Dashpot plant with two parametric uncertainties was designed using the mixed-μ synthesis tools. The closed-loop transfer function was shaped by the compensator to meet the stability- and performance-robustness requirements in the frequency-domain. It was observed that the mixed-μ synthesis compensator achieved good performance-robustness and stability-robustness for the given plant.

Best performance and disturbance-rejection is obtained

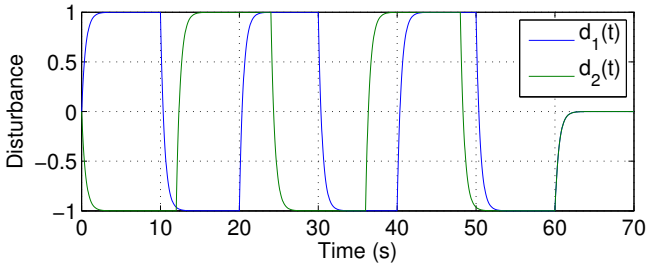

Fig. 13. Filtered Square Wave disturbance

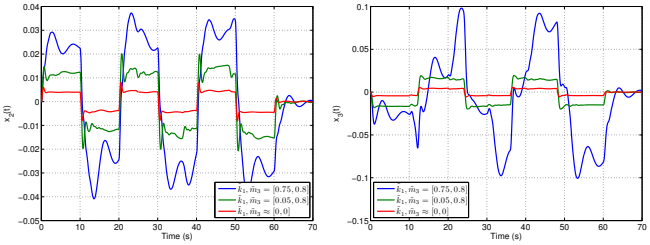

(a) Mass 2 Position (b) Mass 3 Position

Fig. 14. Mass position (Filtered Square Wave disturbance, $A_1 = A_2$)

for smaller uncertainties, while very large uncertainties degrade the closed-loop performance. The directionality of the closed-loop transfer function is shaped by the performance weights. Also, performance weights show that mass 2 position is more difficult to control than mass 3 position, as expected from an engineering perspective.

The commercially available complex-μ D-K iterations yield very conservative performance for real parametric uncertainties. From the users point of view, D-K and D,G-K software uses the same configuration parameters, which makes mixed-μ highly appealing for robust controller synthesis.

Some important questions arise for future work. The generalization of the mixed-μ synthesis to non-linear systems is an exciting and complex problem. Also, a more deep and consistent theoretical basis is required to study which uncertain parameters are most relevant for the μ-synthesis.

REFERENCES

[1] G.J. Balas, J.C. Doyle, K. Glover, A. Packard, and R. Smith. *μ-Analysis and Synthesis Toolbox*. The Mathworks, June 2004.

[2] G.J. Balas and A. Packard. The structured singular value (μ) framework. In *The Control Handbook*, chapter 42, pages 671–687. CRCPress, 1996.

[3] D. Barros, S. Fekri, and M. Athans. Robust Mixed-μ Synthesis Performance For A Mass-Spring Benchmark System. In *Proceeding of the 2005 IEEE International Symposium on Intelligent Control, Mediterranean Conference on Control and Automation*, Limassol, Cyprus, June 2005.

[4] S. Skogestad and I. Postlethwaite. *Multivariable Feedback Control: Analysis and Design*. Wiley, 2nd edition, September 2005.

[5] K. Zhou and J.C. Doyle. *Essentials of Robust Control*. Prentice Hall, September 1997.